Indian Journal of Biochemistry & Biophysics
Vol. 62, December 2025, pp. 1417-1428
DOI: 10.56042/ijbb.v62i12.18514

Study of antibacterial and photocatalytic potential of phytomediatically synthesized ZnO nanoparticles from *Prunus domestica* L.

Kishan[1]*, Rishi Kumar Shukla[1]*, Abha Shukla[2] & Sahil Kumar[3]

[1]Department of Chemistry, Gurukula Kangri (Deemed to be University), Haridwar-249 404, Uttarakhand, India

[2]Department of Chemistry, Kanya Gurukula Campus, Gurukula Kangri (Deemed to be University), Haridwar-249 404, Uttarakhand, India

[3]Department of Botany and Microbiology, Gurukula Kangri (Deemed to be University), Haridwar-249 404, Uttarakhand, India

Received 03 April 2025; *revised 11 May 2025*

Zinc oxide nanoparticles (ZnONPs) are anticipated to be one of the three most commonly produced nanomaterials, alongside TiO_2 and SiO_2 nanoparticles. Many methods are used to synthesize the ZnONPs that affect their precise chemical and physical characteristics. Phyto-mediated synthesis of ZnONPs is one of the most emerging methods nowadays. In the current study, powder of the seed coat of *Prunus domestica* L. is extracted using different solvents, namely Petroleum ether (PE), Diethyl ether (DEE), Ethyl acetate (EA), Methanol (MeOH) and Distilled water (DW). The EA extract has shown the highest antibacterial activity among all the extracts with a zone of inhibition of 24 mm against *P. aeruginosa*. The EA extract of the seed coat of *P. domestica* is further utilized to synthesize the ZnONPs, regarded as PDEA-ZnONPs. The Ultraviolet-visible (UV-Vis), Fourier transformation infrared (FTIR), X-ray diffraction (XRD) and Field emission-scanning electron microscopy (FE-SEM) spectroscopic techniques are used to characterized the synthesized PDEA-ZnONPs. The morphology of PDEA-ZnONPs is found to be spherical with hexagonal wurtzite structure. The average crystallite size of PDEA-ZnONPs is found to be 23.485 ± 6.446 mm. The PDEA-ZnONPs are further utilized in the photocatalytic degradation of Methylene blue (MB) and Methyl orange (MO) dyes. The results of photocatalytic degradation of both the dyes displayed impressive degradation of MB and MO with 88.469 and 91.065 % in 300 min, respectively. Further, the synthesized PDEA-ZnONPs have shown the best antibacterial activity against *E. coli* and *S. aureus* with 28 mm zones of inhibition each.

Keywords: Antibacterial activity, Methyl orange, Methylene blue, Nanoparticles, *Prunus domestica* L., Zinc oxide

In the twenty-first century, nanotechnology emerged as a scientific accomplishment. This field encompasses several disciplines and deals with the synthesis, handling and use of materials smaller than 100 nm called nanoparticles (NPs). NPs are divided into various categories namely zero-dimensional (nanoparticles and quantum dots), one-dimensional (nanorods, nanofibers, nanopillars and nanowires), two-dimensional (nanosheets, nanoplates and nanopores) and three-dimensional (nanocomposites and complex hierarchical structures) depending on their morphology[1, 2].

The environment, agriculture, food, biotechnology, biomedical, pharmaceutical and many other fields benefit greatly from the use of NPs[3]. NPs with biological uses can be synthesized by the process called biosynthesis, which involves the use of microorganisms and plants. This strategy is safe, affordable, biocompatible, green and environmentally friendly[4]. Advanced features of NPs include targeted drug delivery, hyperthermia, photoablation therapy, bioimaging, bio-sensoring, antimicrobial, anticancer, anti-inflammatory activity. The tumour-targeting attributes of NPs have spurred a rise in the biotechnological and applied microbiological applications of NPs[5-8].

The natural phytochemicals present in plant extract obtained from different parts of plants (like roots, leaves, stems, seeds and fruits) act as reducing, capping or stabilization agents. NPs synthesized via a green approach (*i.e.*, phyto-mediated synthesis) show more catalytic activity and limit the use of expensive and toxic chemicals[9].

In the textile and apparel sectors, dyes (*i.e.*, organic substances) are used for colouring purposes. Usually, they are categorized according to the particle charge produced when they are dissolved in an aqueous medium. Their primary classifications were natural and synthetic dyes, which were further subdivided into anionic, cationic and non-ionic dyes based on their charges during ionization. Due to the

*Correspondence:
E-mail: prajapatikishan75@gmail.com (Kishan);
rkshukla@gkv.ac.in (RKS)

intricate structures, most of the dyes are stable and difficult to degrade[10,11]. According to studies on dye toxicity, dyes may cause significant harm to aquatic life even at low concentrations. This is mostly because they degrade slowly through oxidation, hydrolysis, physical contact and chemical interactions, releasing harmful compounds. Furthermore, dyes negatively impact aquatic life by preventing light from entering the water system and decreasing the photosynthetic reaction. In addition, because dyes have mutagenic and carcinogenic properties, they are harmful to humans, animals and aquatic life[12].

In recent studies, numerous inorganic metal oxides NPs, such as ZnO, CuO and TiO_2 have been synthesized. Among these, ZnONPs are the most interesting due to their low cost of production, safety and ease of preparation[13]. There have been reports on ZnONPs that depict the variation in the morphologies of ZnONPs, including nanoflake, nanoflower, nanobelt, nanorod and nanowire[9]. The ZnONPs exhibit tremendous catalytic, anti-inflammatory, wound healing, anti-cancer, anti-diabetic, antibacterial, antifungal activities, making them valuable in various medicinal applications[9,14-18]. Even though ZnONPs are also used for targeted delivery of medicines[19].

There are many methods described in literature to synthesize the ZnONPs such as laser ablation, hydrothermal technique, electrochemical depositions, sol-gel technique, chemical vapor deposition, thermal decomposition, combustion techniques, ultrasound assisted technique, microwave-assisted combustion technique, two-step mechanochemical–thermal synthesis, anodization, co-precipitation and electrophoretic deposition[20]. The ZnONPs with different morphologies can be synthesized by controlling the parameters of the precipitation process, *e.g.*, solution concentration, pH and washing medium[21]. Phyto-mediated synthesis of ZnONPs is one of the most emerging methods nowadays.

Plum (or *Prunus domestica* L.) is a member of the Rosaceae family. Its fruit, which may be eaten fresh or dried, is used as food and medicine. Eating *P. domestica* fruit has been linked to several medical advantages, including improved blood circulation, immunity to measles and relief from stomach issues[22]. Chlorogenic acids, anthocyanins, flavanols and coumarins are the principal polyphenolic substances found in *P. domestica*. Several reports have demonstrated that the fruit of *P. domestica* possesses numerous noteworthy pharmacological activities, including antioxidant, antihyperlipidemic, anticancer, anti-osteoporosis, anxiolytic, antibacterial and memory-boosting attributes[23].

Thus, keeping the above advantages of *P. domestica* and ZnONPs in view, first we carried out the antibacterial activity to find the most promising extract of the seed coat of *P. domestica*. Then, we synthesized the ZnONPs using the EA extract and characterized using different spectroscopic techniques. Further, we performed the antibacterial activity and photocatalytic activity (dye degradation potential) of PDEA-ZnONPs using MB and MO dyes.

Materials and Methods

Sample Collection and Authentication

The fruits of *P. domestica* were purchased from the orchards located in Haridwar, Uttarakhand (India). The Botanical Survey of India (BSI), Dehradun, has identified and verified the plant under the accession number 374.

Chemicals and Reagents

Petroleum ether (SD fine), Diethyl ether (SD fine), Ethyl acetate (SD fine), Methanol (CDH), 2, 2-diphenyl-1-picrylhydrazyl (DPPH) (Sigma-Aldrich), Zinc acetate dihydrate (Fisher), DMSO (CDH), Methylene blue (Sigma-Aldrich) and Methylorange (Sigma-Aldrich). The chemicals used in the study were all analytic grade.

Extract Preparation

Briefly, 200 g of the seed coat powder of *P. domestica* was put into the Soxhlet extractor. Approximately 72 cycles of siphoning were carried out using PE, DEE, EA, MeOH and DW (or the process was carried out until the siphoning tube looked colourless). The extracts were filtered to remove particulate matter. Then, the extracts were concentrated using a rotary evaporator under reduced pressure and the concentrated extracts were stored in the refrigerator until further examination[24].

Antibacterial Activity of the Various Extracts and PDEA-ZnONPs

The antibacterial activity was performed by the agar-well diffusion method[25]. The antibacterial activity was assessed using four Gram-negative bacteria (*E.coli, S. typhi, K. Pneumonia* and *P. aeruginosa*) and three Gram-positive bacteria (*L. monocytogenes, S. aureus* and *S. pyogenes*). For the test microorganisms, Muller Hinton Broth and

Muller Hinton Agar (MHA) were utilized as cultures. Petri plates were filled with the sterilized MHA, which were then allowed to solidify for a while. On MHA plates, fresh overnight cultures of every strain were equally swabbed, having turbidity equal to the McFarland standard (0.5). Following that, a cork borer was used to pierce the wells in the Petri plates. 200 µL of each extract solution (100 mg/ml of extracts/PDEA-ZnONPs in DMSO) was then added to the wells and left to incubate for 24 h at 37°C. Commercially available discs of Gentamicin 30 µg and Chloramphenicol 25 µg served as standards, *i.e*., positive controls, while the negative control was DMSO. The whole test procedure of antibacterial activity was performed in laminar air flow (LAF).

Zinc Oxide Nanoparticles Using the Ethyl Acetate Extract of Seed Coat of *P. domestica* (*i.e*., PDEA-ZnONPs)

Based on the antibacterial activity, we selected the EA extract for the synthesis of ZnONPs. PDEA-ZnONPs were synthesized using Zinc acetate dihydrate [$Zn(OAc)_2.2H_2O$] as the precursor. Briefly, 100 ml of 0.6 M MeOH was used to dissolve 13 g of [$Zn(OAc)_2.2H_2O$]. 400 mg of EA extract of the seed coat was added to this and stirred for 3 h. The solution was filtered and the filtrate was titrated with 10% NH_3 solution until the precipitation stopped. The precipitate was filtered and washed with hot water to remove the excess NH_3. To dry out the precipitate, left it for a whole night at 105°C. Following that, the dried precipitate was calcined at 400°C for 4 h[26, 27].

Characterization of Synthesized PDEA-ZnONPs

The absorption spectrum of PDEA-ZnONPs was measured using a UV-Vis-NIR spectrophotometer (Shimadzu, UV-3600) at a resolution of 0.5 nm to validate their fabrication. The Fourier transform infrared spectroscopy (FTIR) spectrum was recorded in the region from 400 to 4000 cm^{-1} range (Perkin Elmer, FTIR spectrum version 10.4.00 by KBr pellet method). The crystal structure investigation of the fabricated PDEA-ZnONPs was done by the powder X-ray diffraction (p-XRD) pattern recorded on the Xray diffractometer (Panalytical X-Pert Pro) in continuous scan mode from 5º to 100º of 2θ. Field emission-scanning electron microscopy (FE-SEM) was used to assess the size and morphology of the fabricated PDEA-ZnONPs (FE-SEM Supra 55, Karl Zeiss).

UV-Assisted Dye Degradation Activity (Methylene Blue-MB and Methyl Orange-MO)

Photocatalytic performance of the synthesized PDEA-ZnONPs was evaluated under UV-light illumination[28]. Briefly, 0.09 g of ZnONPs was dispersed in 150 mL of 20 µM MB and MO dye solutions. Preceding to the photocatalytic experiment, dye solutions with PDEA-ZnONPs were subjected to stirring in the dark for 1 hour to attain adsorption-desorption equilibrium. During the stirring in the dark, 5 mL of each dye solution was withdrawn and the absorbance was recorded using UV–Vis Spectrophotometer (Systronics–2205). Then, the dye solutions with PDEA-ZnONPs were kept under UV light and changes in concentrations of the dye solutions were recorded at different time intervals. The degradation percentage of dye solutions was calculated by the following equation:

$$\% \text{ dye degradation} = \frac{\text{Abs (control)} - \text{Abs (sample)}}{\text{Abs (control)}} \times 100$$

Results and Discussion

Antibacterial Activity of Different Extracts of Seed Coat

The antibacterial activity was tested against the three Gram-positive and four Gram-negative bacteria. The Gram-positive and Gram-negative bacteria can be differentiated by their morphology. The fundamental features of Gram-positive cell walls include a thick coating of peptidoglycan and the absence of an outer membrane; instead of lipopolysaccharides, these consist of teichoic acid and lipoteichoic acid localized in the cell wall of bacteria[29]. The Gram-negative bacteria have a thin cell wall of peptidoglycan. In addition to an inner membrane, they also have an outer membrane, which contains lipids and is separated from the cell wall by the periplasmic space filled with periplasmic enzymes and binding proteins[30, 31]. The results of the antibacterial activity of the different extracts of the seed coat are depicted in (Table 1, and Figs 1 & 2) show the Petri-plates and (Fig. 3) depicts the graphical representation of the antibacterial activity of different extracts. All the extracts of seed coat have shown good antibacterial activity against all the tested bacterial strains except the aqueous extract, which did not show antibacterial activity against *S. pyogenes*. The EA extract has shown the best antibacterial activity against *P. aeruginosa* (zone of inhibition *i.e.,* ZOI of 24 mm), followed by DEE (ZOI of 21 mm), MeOH (ZOI of 21mm), PE (ZOI of 11 mm) and DW (ZOI of 7 mm).

The amount of the secondary metabolites in the extract is responsible for its optimal antibacterial action. The growth and metabolic activities of bacteria

Table 1 — Antibacterial activity of different extracts of seed coat of *P. domestica*

Bacterial strain	Type	MTCC No.	Zone of inhibition (mm)						
			Standard		Extract				
			Chloramphenicol	Gentamicin	PE	DEE	EA	MeOH	DW
L. monocytogenes	+	MTCC-657	20	17	3	2	7	4	2
S. aureus	+	MTCC-96	21	26	8	14	17	11	3
S. Pyogenes	+	MTCC-442	20	27	5	14	17	8	---
E. coli	-	MTCC-571	25	28	7	11	14	7	4
K. pneumonia	-	MTCC-432	21	27	10	11	21	10	2
P. aeruginosa	-	MTCC-741	26	23	11	21	24	21	7
S. typhi	-	MTCC-98	36	35	7	10	13	14	5

L. monocytogenes = Listeria monocytogenes, S. aureus = Staphylococcus aureus, S. pyogenes = Streptococcus pyogenes, E coli = Escherichia coli, K. pneumonia = Klebsiella pneumonia, P. aeruginosa = Pseudomonas aeruginosa, S. typhi = Salmonella typhi, MTCC = Microbial type culture collection and gene bank, PE = Petroleum ether; DEE = Diethyl ether; EA = Ethyl acetate; MeOH = Methanol and DW = Distilled water

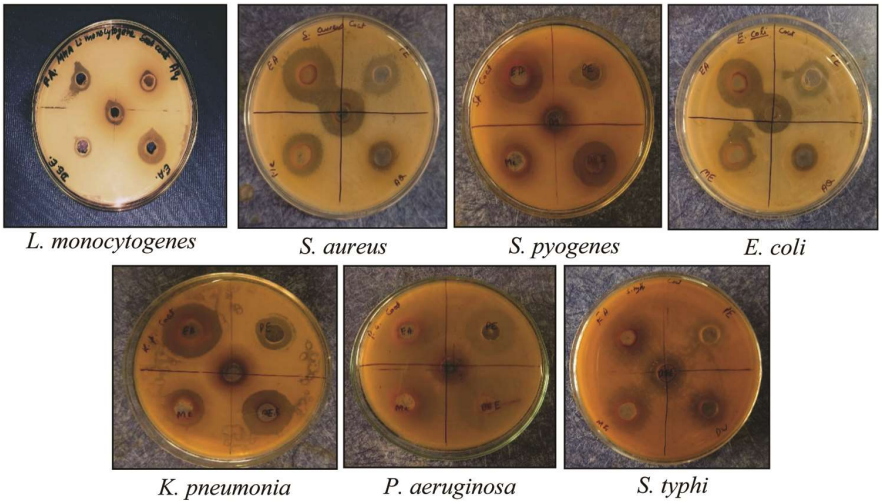

Fig. 1 — Petri-plates of antibacterial activity of different extracts of seed coat of *P. domestica*

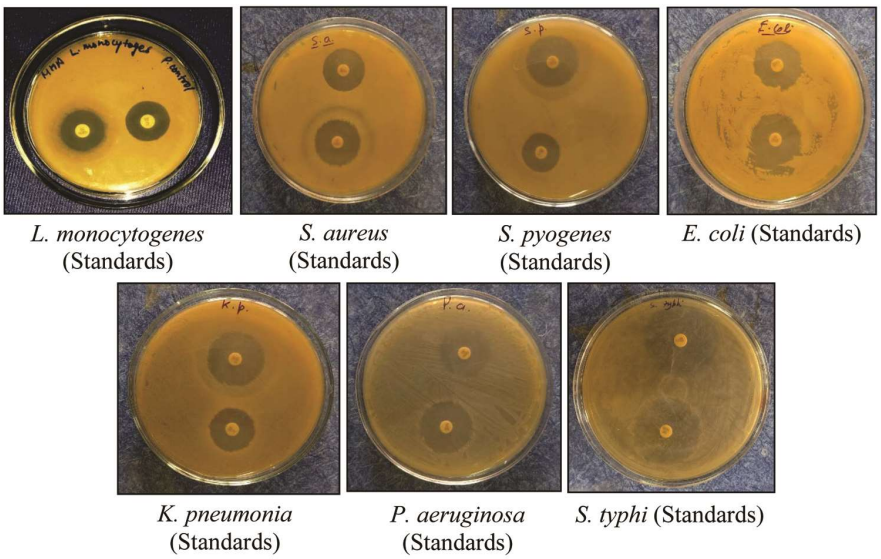

Fig. 2 — Petri-plates of antibacterial activity of Chloramphenicol and Gentamicin

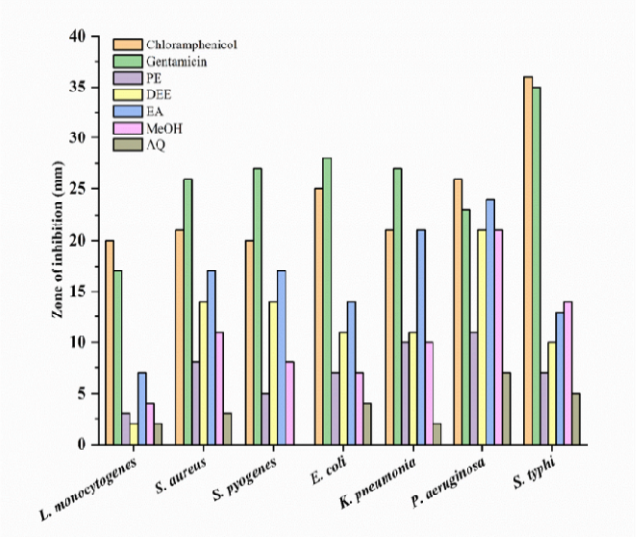

Fig. 3 — Antibacterial activity of different extracts of seed coat of *P. domestica*

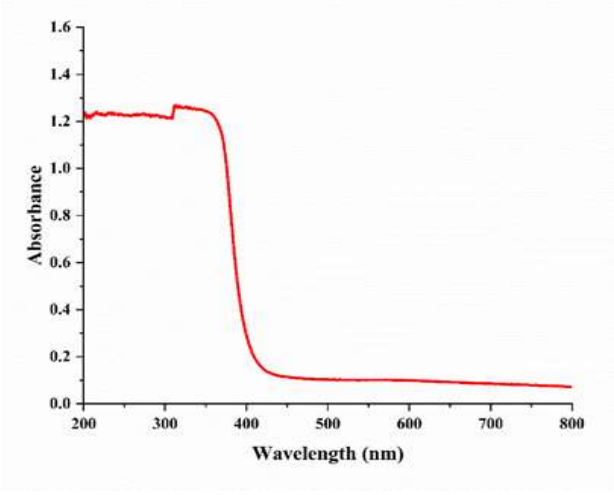

Fig. 4 — UV-Visible spectrum of synthesized PDEA-ZnONPs

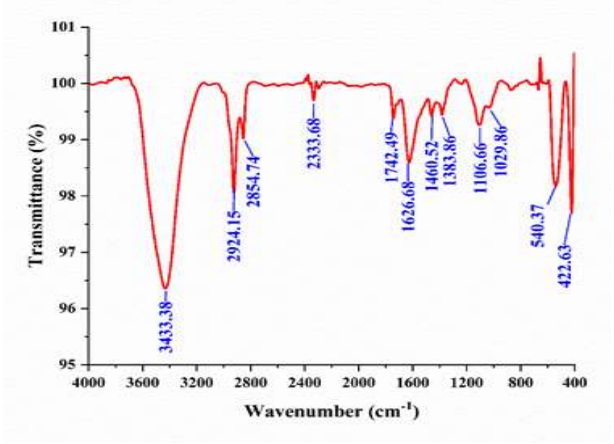

Fig. 5 — FTIR spectrum of synthesized PDEA-ZnONPs

are inhibited by these secondary metabolites[32]. It is challenging to summarize the antibacterial activity of plant extract to a small number of active principles since an extract usually demonstrates the complex combination of secondary metabolites, making the involvement of the other minor metabolites impossible to negate. The antibacterial activity data indicates that the extracts of mid-polar solvent are more active than the most polar solvent and the least polar solvent. Since EA extract has demonstrated the highest antibacterial activity, we have selected it for the manufacture of ZnONPs.

Characterization of Synthesized PDEA-ZnONPs

UV-Visible Spectroscopy

Figure 4 shows the UV-Vis spectrum of the synthesized PDEA-ZnONPs, which is recorded from 200 to 800 nm. The UV-Vis spectrum revealed the surface plasmon resonance (SPR) peak of PDEA-ZnONPs between 311-357 nm. This is in line with the earlier research that found the SPR peak to be between 360 and 380 nm[33]. The bioactive phytochemicals found in the EA extract of the seed coat of *P. domestica* first changed the Zn^{2+} ions into zero-valent Zn atoms. The PDEA-ZnONPs are synthesized when the zero-valent Zn atoms convert the remaining Zn^{2+} ions to ZnO and finally form a cluster structure. Phytochemicals act as capping and stabilizing agents during the manufacture of stable nanomaterials[34]. The biosynthesized PDEA-ZnONPs have shown strong UV absorbance suggesting thatthey are appropriate for use in UV protection applications[35]. The energy band gap (Ebg) of the synthesized PDEA-ZnONPs ranged between 3.47 and 3.98 eV, which is calculated by using the equation Ebg = 1240/λ eV, where λ is the wavelength in nm[36]. In another investigation, the Ebg was found to be 3.33 and 3.39 eV, respectively, for ZnONPs synthesized by utilizing the *Cassisa fistula* and *Peltophorum pterocarpum* leaf extract[37, 38]. Hence, the UV-Vis spectroscopy results are quite consistent with the researches that have already been published.

FTIR (Fourier Transform Infrared) Spectroscopy

The FTIR technique is used to study the various functional groups of plant extract that were involved in the synthesis (*i.e*., stabilizing and reducing) of PDEA-ZnONPs. The FTIR spectrum of PDEA-ZnONPs is displayed in (Fig. 5). Various bands at 3433.38 cm^{-1} (OH stretching of carboxylic acid or phenol), 2924.15cm^{-1} (C-H stretching of alkyl group)[39,40], 2333.68 cm^{-1} (CN stretching nitrile)[37], 1742.49 cm^{-1} (C=O of stretching),

Table 2 — Miller indices, full width half maxima (FWHM), peak positions and average crystallite size of PDEA-ZnONPs

Miller indices (hkl)	FWHM (degree)	Peak position (2θ in degree)	Crystallite size (nm)
100	0.4133	31.978	20.4
002	0.3838	34.605	22.1
101	0.4133	36.474	20.7
102	0.3542	47.684	25.1
110	0.4428	56.784	20.8
103	0.4723	63.044	20.1
200	0.5314	66.516	18.2
112	0.3247	68.204	30.3
201	0.4723	69.250	20.8
004	0.2952	72.772	34.4
202	0.2952	77.018	35.4
104	0.8266	81.633	12..8
203	0.4723	89.857	24.2
	Average crystallite size		23.485 ± 6.441 nm

Average crystallite size is represented as mean ± standard deviation.

1626.68 cm^{-1} (NH bending of amide or amine), 1383.86 cm^{-1} (N-O stretch of nitro compound or weak C-H rocking of alkane), 1029.86 cm^{-1}(C-O stretch of alcohol, carboxyl or ether)[35,39,41], 540.37 and 422.63 cm^{-1} (metal oxide or Zn-O vibrations)[27,35,37] are appeared in the FTIR spectrum of PDEA-ZnONPs. These unique bands thus imply that a variety of biomolecules found in the EA extract of the seed coat of *P. domestica* were involved in the synthesis of PDEA-ZnONPs[42]. There are several advantages of fabricating the NPs using natural plant extract. One such advantage is that the pharmacological entities, including phenolic and polyphenolic compounds, can be coated on the metal oxide layer of the NPs[35]. During the synthesis process, carboxylic, amino and phenolic acids are essential for bio-capping. They also interact with the ZnONPs surface and help to stabilize the ZnONPs[39]. This allows the NPs to connect with their receptors on the bacterial membranes[35].

XRD (X-Ray Diffractometry)

As can be seen in Figure 6, the XRD pattern produced by PDEA-ZnONPs offers an unambiguous description of their crystalline structure. Table 2 demonstrates the Miller indices (hkl), full width half maxima (FWHM), peak position and crystallite size of the synthesized PDEA-ZnONPs. Different diffraction peaks are appeared at 2θ values of 31.978, 34.605, 36.474, 47.684, 56.784, 63.044, 66.516, 68.204, 69.250, 72.772, 76.018, 81.633 and 89.857 degrees. These peaks have the miller indices (*i.e.*, diffraction lattice planes) corresponds to (100), (002), (101), (102), (110), (103), (200), (112), (201), (004), (202), (104) and (203), respectively. This demonstrates that the synthesized PDEA-ZnONPs have a hexagonal wurtzite structure.

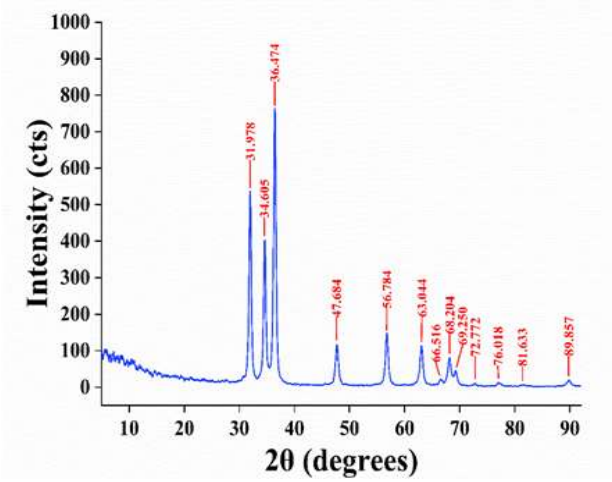

Fig. 6 — XRD pattern of synthesized PDEA-ZnONPs

Figure 7 shows the XRD pattern that corresponds to the Joint Committee on Powder Diffraction Standards (JCPDS) card number 96-210-7060. The synthesized PDEA-ZnONPs have shown an average crystallite size of 23.485 ± 6.441 nm and it was calculated using the Debye-Scherer equation as below[43, 44]:

$$D = \frac{K\lambda}{\beta Cos\theta}$$

Where: D = Crystal size, λ = X-ray wavelength coming from Cu-K_α (0.1540560 nm), θ = Bragg's diffraction angle, K = Shape factor or Scherrer constant (0.89) and β = Full width at half maxima of the diffraction peak in radian.

FE-SEM (Field Emission-Scanning Electron Microscopy)

The FE-SEM images of the fabricated PDEA-ZnONPs are displayed in (Fig. 8), which make it clear

that the synthesized PDEA-ZnONPs have a spherical shape. Using ImageJ software, the average diameter of PDEA-ZnONPs is measured to be 41.713 ± 6.796 nm. The hexagonal structure of the fabricated PDEA-ZnONPs is determined by XRD examination. This clarifies the overall morphology of nanoparticles to be spherical hexagonal wurtzite. The physical appearance of the NPs determines how well they fight infections. Spherical nanoparticles offer a more potent antibacterial impact because of their ability to easily penetrate the pathogen cell wall. Furthermore, the large surface area of spherical NPs shows promise as a practical material for dye removal (waste water treatment)[45]. The ZnO nanorods have been the focus of much study because of their exceptional versatility in a variety of fields, such as solar cells, sensors, photo detectors, photocatalysts and microchip technology[46].

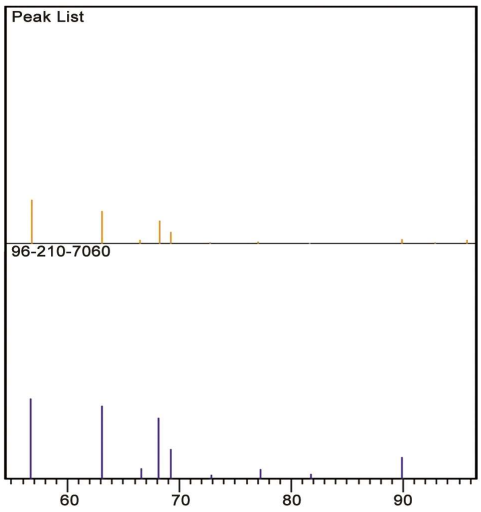

Fig. 7 — JCPDS card number matching of synthesized PDEA-ZnONPs

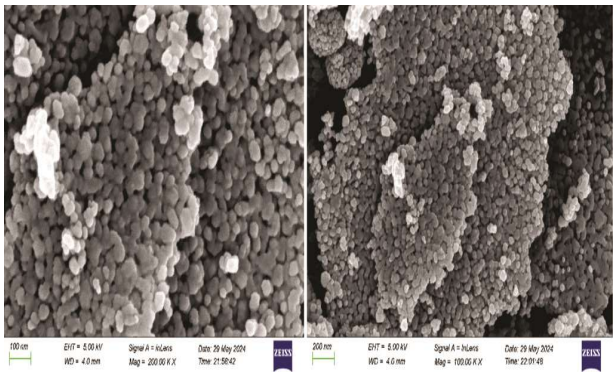

Fig. 8 — FE-SEM images of synthesized PDEA-ZnONPs

Photocatalytic Performance

The synthesized PDEA-ZnONPs are used as a photocatalyst for the degradation of MB and MO dyes under direct UV-light illumination. The mechanism for the photodegradation of MB and MO dyes in the presence of PDEA-ZnONPs can be clarified as follows:

$$ZnO + h\nu \rightarrow ZnO\ (h^{+}_{vb} + e^{-}_{cb})$$

$$OH^{-}_{ads} + h^{+}_{vb} \rightarrow OH^{\cdot}_{ads}$$

$$MB/MO + OH^{\cdot}_{ads} \rightarrow \text{Degradation of dye}$$

The formation of an electron (e^{-}) in the conduction band and a hole (h^{+}) in the valence band occur when radiation of a certain energy strikes the catalyst surface with enough energy to match or exceed the band gap energy. Water is oxidized by the hole to form OH radicals and the oxygen adsorbed on the catalyst is reduced by the electron in the conduction band[38].

The absorption spectra of photocatalytic suspensions are recorded under dark and UV-light illumination conditions are shown in (Figs 9 and 10) for MB (λ_{max}= 764 nm) and MO (λ_{max}= 464 nm),

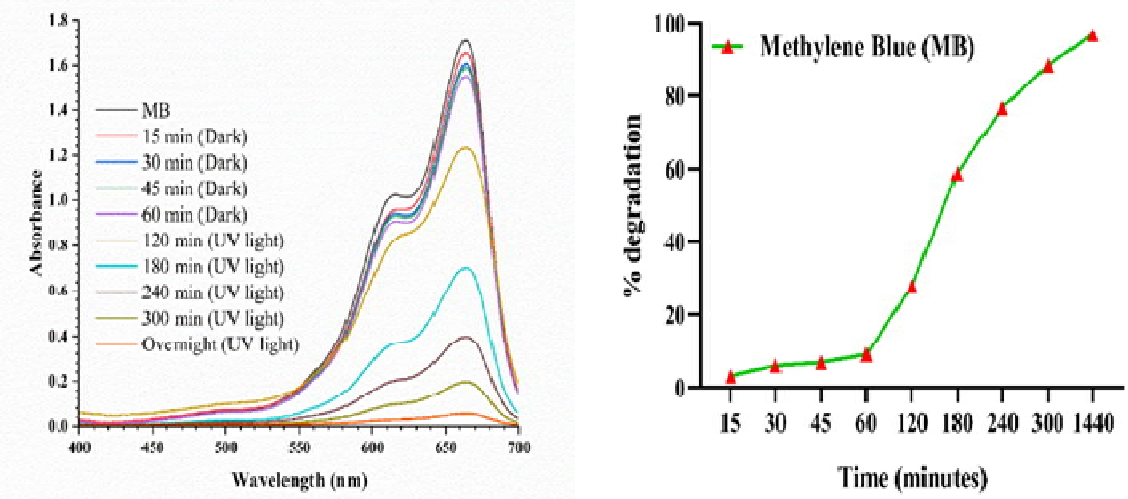

Fig. 9 — Time dependent UV-Vis absorption spectra and time dependent % degradation of MB by synthesized PDEA-ZnONPs

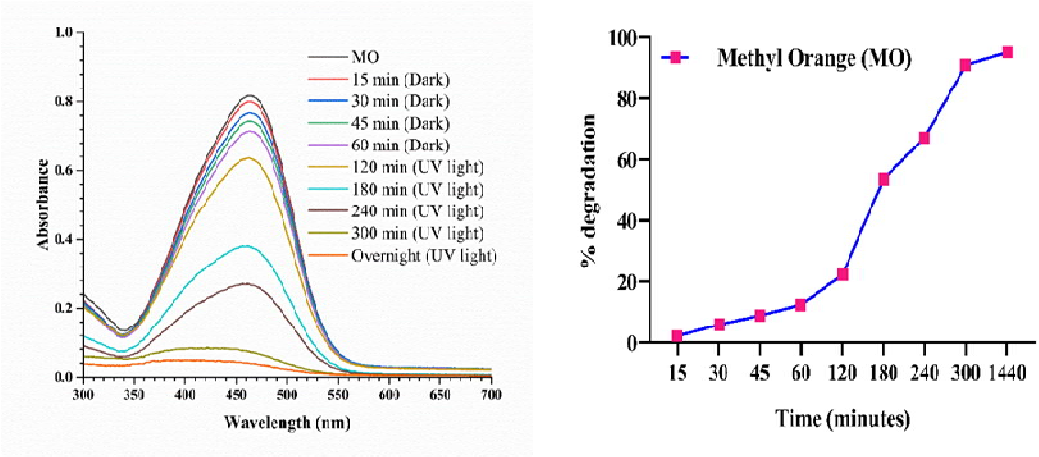

Fig. 10 — Time dependent UV-Vis absorption spectra and time dependent % degradation of MO by synthesized PDEA-ZnONPs

respectively. It can be observed from (Fig. 9) that photocatalyst PDEA-ZnONPs under the dark conditions with MB unveiled a slight decline in concentration as a consequence of adsorption of MB on the surface of PDEA-ZnONPs. During the experiment, only a slight portion (up to 8.963 %) of MB was degraded in the dark. As the MB dye solution with PDEA-ZnONPs was exposed to the UV-light, the degradation of MB dye was 88.469% and 98.788 % after 300 min and overnight, respectively. Our findings demonstrate the time-dependent dye degradation under UV light as reported in some previous reports[28]. In a previous study, ZnONPs synthesized using *Artocarpus gomezianus* showed 81% degradation of MB in 100 min under sunlight conditions[47]. It is evident from Figure 10 that under the dark conditions, up to 12.485 % degradation of MO dye took place. As the MO dye solution with PDEA-ZnONPs was exposed to UV-light, the degradation was 91.065 and 95.226 % after 300 min and overnight, respectively. In a previous report, MO dye degraded up to 92.10 % under solar illumination by the Fe-doped ZnONPs synthesized using wild olive leaf extract[48]. The variations of % degradation of the MB and MO dyes concerning time are depicted in (Table 3). This study reveals the good photocatalytic performance of the synthesized PDEA-ZnONPs by degrading the MB and MO dyes, which are tremendously toxic to human beings. The synthesized PDEA-ZnONPs may also be effective in the purification of the water as these NPs have efficiently degraded the MB and MO dyes.

Table 3 — Degradation (%) of MB and MO by synthesized PDEA-ZnONPs

Time (min)	Degradation (%)	
	MB	MO
15	3.163	2.203
30	5.917	5.998
45	6.913	8.935
60	8.963	12.485
120	27.837	22.277
180	58.827	53.611
240	76.743	67.197
300	88.469	91.065
1440 (Overnight)	96.788	95.226

Kinetics of the Photochemical Reaction

The kinetics of the photochemical degradation of the MB and MO by the PDEA-ZnONPs was estimated using the pseudo-first-order kinetic equation:

$$-\ln(C_t/C_0) = kt + b$$

Where: C_t is the concentration of MB and MO at time 't' after completing the photochemical reaction in UV light, C_0 is the initial concentration of MB and MO, k is the photochemical reaction rate constant, t is the time of the reaction and b is a constant. The graphs are found to be linear in the time range 120 – 300 min, which resembles the pseudo-first-order kinetics. Figures 11 and 12 show the graphical representation of $-\ln(C_t/C_0)$ *vs* t for MB and MO, respectively. Table 4 shows the value of rate constants of the photocatalytic degradation of MB and MO. The rate constants for the degradation of MB and MO are found to be $k_{MB} = 1.7 \times 10^{-4}$ and $k_{MO} = 1.9 \times 10^{-4}$ sec^{-1}, respectively. In a previous study, the rate constant for the photocatalytic degradation of MB is reported to be 10.8×10^{-4} (sec^{-1})[28].

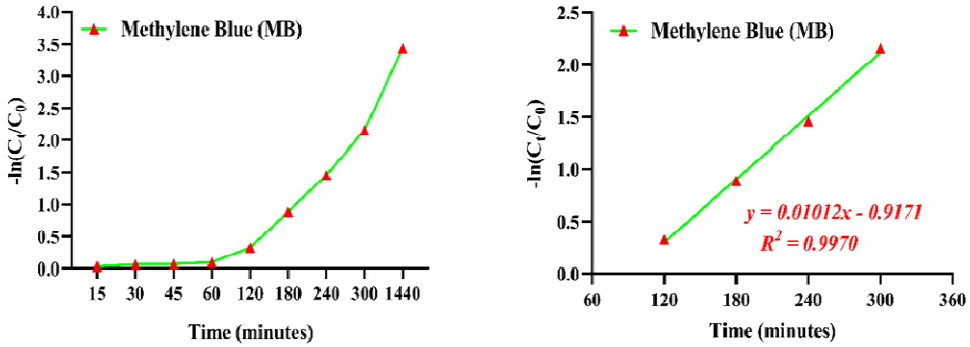

Fig. 11 — Graphical representation of $-\ln(C_t/C_0)$ *vs* time for MB

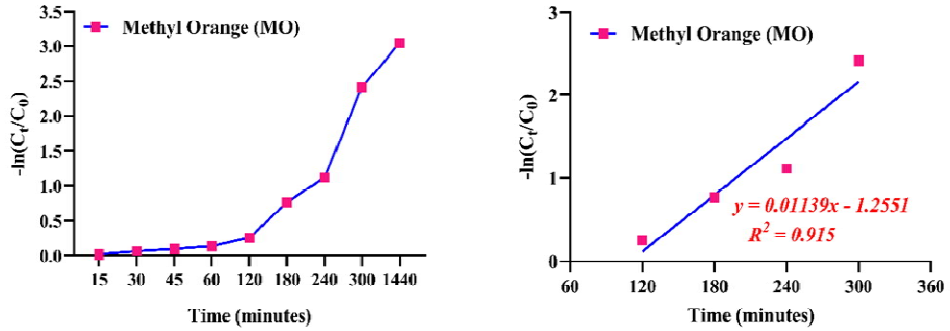

Fig. 12 — Graphical representation of $-\ln(C_t/C_0)$ *vs* time for MO

Table 4 — Rate constants of MB and MO degradation by the synthesized PDEA-ZnONPs

Rate constant	sec^{-1}
k_{MB}	1.7×10^{-4}
k_{MO}	1.9×10^{-4}

k_{MB} = rate constant for the degradation of MB and k_{MO}= rate constant for the degradation of MO.

Antibacterial Activity of PDEA-ZnONPs

The results of the antibacterial activity of the synthesized PDEA-ZnONPs are depicted in (Table 5). Figure 13 shows the Petri-plates and Figure 14 depicts the graphical representation of the antibacterial activity of the synthesized PDEA-ZnONPs. The synthesized PDEA-ZnONPs have shown decent antibacterial activity against all the tested pathogens. For Gram-positive bacteria, the synthesized PDEA-ZnONPs have shown the highest ZOI of 28 mm against *S. aureus,* followed by *L. monocytogenes* and *S. pyogenes* with ZOI of 21 and 20 mm, respectively. For Gram-negative bacteria, the synthesized PDEA-ZnONPs have shown the highest ZOI of 28 mm against *E. coli,* followed by *P. aeruginosa, S. typhi* and *K. pneumonia* with zone of inhibition of 25, 25

Table 5 — Antibacterial Activity of the synthesized PDEA-ZnONPs

Bacterial Strain	Type	MTCC No.	Zone of Inhibition (mm)
L. monocytogenes	+	MTCC-657	21
S. aureus	+	MTCC-96	28
S. pyogenes	+	MTCC-442	20
E. coli	-	MTCC-571	21
K. pneumonia	-	MTCC-432	23
P. aeruginosa	-	MTCC-741	25
S. typhi	-	MTCC-98	25

L. monocytogenes = *Listeria monocytogenes, S. aureus* = *Staphylococcus aureus, S. pyogenes* = *Streptococcus pyogenes, E coli* = *Escherichia coli, K. pneumonia* = *Klebsiella pneumonia, P. aeruginosa* = *Pseudomonas aeruginosa, S. typhi* = *Salmonella typhi* and MTCC = Microbial type culture collection.

and 23 mm, respectively. In early research, the antibacterial activity of ZnONPs was carried from 50 to 400 µg/mL, and it demonstrated that the ZOI varied from 0 to 22.67 mm for *E. coli*, 0 to 20.87 mm for *S. aureus*, 0 to 18.57 mm for *P. aeruginosa* and 0 to 21.47 mm for *K. Pneumonia* in a dose dependant manner[49]. The antibacterial activity of ZnONPs against *S. typhi* was assessed in an early investigation at five concentrations: 0.625, 1.25, 2.5, 5 and

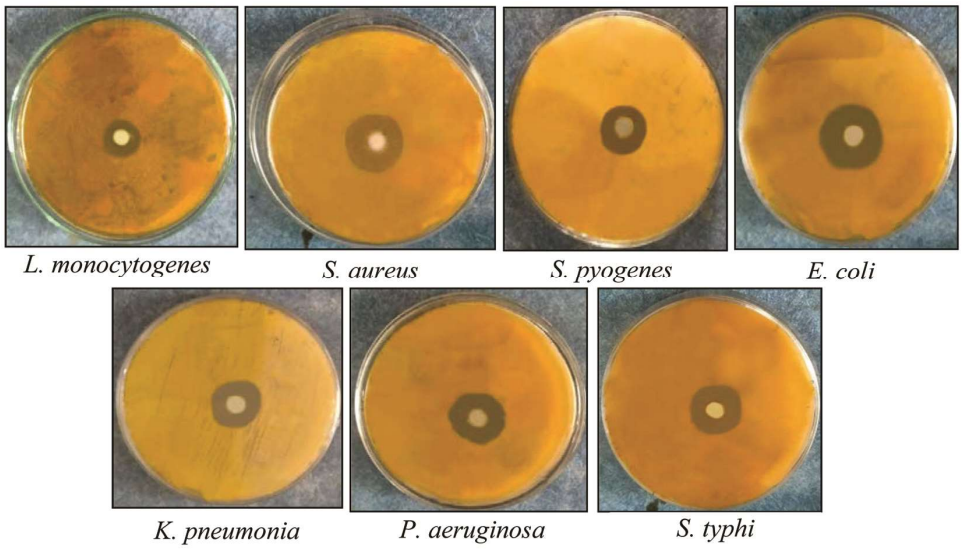

Fig. 13 — Petri-plates of antibacterial activity of PDEA-ZnONPs

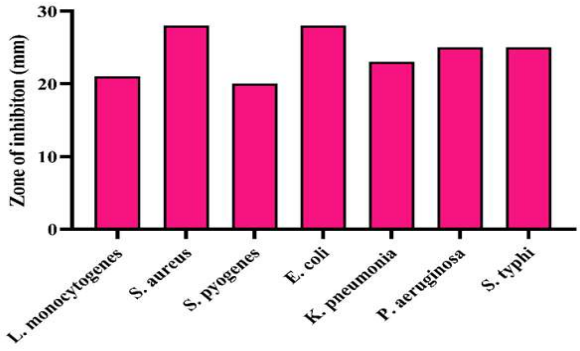

Fig. 14 — Antibacterial activity of the synthesized PDEA-ZnONPs

10 mg/mL, correspond to 16, 18, 20, 28 and 31 mm of ZOI[50]. In prior research, the agar well diffusion technique demonstrated dose-dependent antibacterial activity against *L. monocytogenes* at different concentrations (0.05, 0.10, 0.50 and 1 mg/mL) of ZnONPs synthesized using leaf extract of *Raphanus sativus*[51]. The ZnO nanosheets synthesized using the aqueous leaf extract of *Phyllanthus emblica* checked at different concentrations 30, 50 and 100 µg/mL for their antibacterial activity against *S. pyogenes* showed a dose dependant response with ZOI of 9, 12 and18 mm, respectively[52]. From above discussion, it can be concluded that the phytochemicals present in the different extracts are primarily responsible for the exceptionally good varied antibacterial activity of ZnONPs. This is certainly the reason for the decent antibacterial activity of PDEA-ZnONPs.

Conclusion

In summary, the phyto-mediated synthesis of PDEA-ZnONPs is successfully carried out using the EA extract of the seed coat of *P. domestica.* The synthesized PDEA-ZnONPs are characterized by UV-Vis, FTIR, XRD and FE-SEM techniques. UV-vis spectroscopy showed the SPR peak between 311-357 nm. The FTIR spectrum showed the presence of different functional groups, *e.g.*, -COOH, -OH, -CN, $-NH_2$, $-NO_2$, Zn-O, *etc*. The XRD analysis confirmed the structure of PDEA-ZnONPs to be hexagonal wurtzite. The shape of the PDEA-ZnONPs is found to be spherical by the FE-SEM analysis. Further, the PDEA-ZnONPs were analyzed for UV-assisted photocatalytic activity using MB and MO dyes. The synthesized PDEA-ZnONPs have shown nice dye degradation activity, which shows the significance of the synthesized PDEA-ZnONPs for the treatment of water for the removal of the toxic substances (MB and MO). Against the Gram-positive and Gram-negative bacterial pathogens, the synthesized PDEA-ZnONPs have demonstrated a broad spectrum of antibacterial activity. These results provide credence to the idea that the PDEA-ZnONPs may be a promising option for medicinal and biological applications. In the era of antimicrobial resistance, the use of NPs to attack bacterial infections could be a viable and effective technique.

Acknowledgement

The authors are thankful to Department of Chemistry, GK(DU), Haridwar, Uttarakhand, for

providing experimental facilities. The authors are thankful to Material Research Centreat MNIT, Jaipur, Rajasthan, along with Central Building Research Institute-CSIR, Roorkee, for carrying out the FTIR, XRD and FE-SEM analyses.

Conflicts of interest

All authors declare no conflicts of interest.

References

1 Byakodi M, Shrikrishna NS, Sharma R, Bhansali S, Mishra Y, Kaushik A & Gandhi S, Emerging 0D, 1D, 2D and 3D nanostructures for efficient point-of-care biosensing. *Biosens Bioelectron: X*, 12 (2022) 100284.

2 Khan I, Saeed K & Khan I, Nanoparticles: Properties, applications and toxicities. *Arab J Chem*, 12 (2019) 908.

3 Altammar KA, A review on nanoparticles: Characteristics, synthesis, applications and challenges. *Front Microbiol*, 14 (2023) 1155622.

4 Salam HA, Sivaraj R & Venckatesh R, Green synthesis and characterization of zinc oxide nanoparticles from *Ocimum basilicum* L. var. *purpurascens* Benth.-Lamiaceae leaf extract. *Mater Lett*, 131 (2014) 16.

5 Agarwal H, Nakara A & Shanmugam VK, Anti-inflammatory mechanism of various metal and metal oxide nanoparticles synthesized using plant extracts: A review. *Biomed Pharmacother*, 109 (2019) 2561.

6 Bukhari A, Ijaz I, Gilani E, Nazir A, Zain H, Saeed R, Alarfazi SS, Hussain S, Aftab R & Naseer Y, Green synthesis of metal and metal oxide nanoparticles using different plants' parts for antimicrobial activity and anticancer activity: A review article. *Coatings*, 11(2021) 1374.

7 McNamara K & Tofail SA, Nanoparticles in biomedical applications. *Adv Phys: X*, 2 (2017) 54.

8 Vinardell MP & Mitjans M, Antitumor activities of metal oxide nanoparticles. *Nanomaterials*, 5 (2015) 1004.

9 Agarwal H, Kumar SV & Kumar SR, A review on green synthesis of zinc oxide nanoparticles–An eco-friendly approach. *Resour Eff Technol*, 3 (2017) 406.

10 Yagub MT, Sen TK, Afroze S & Ang HM, Dye and its removal from aqueous solution by adsorption: A review. *Adv Colloid Interface Sci*, 209 (2014) 172.

11 Zhang Z, Moghaddam L, O'Hara IM & Doherty WOS, Congo red adsorption by ball-milled sugarcane bagasse. *Chem Eng J*, 178 (2011) 122.

12 Kefeni KK & Mamba BB, Photocatalytic application of spinel ferrite nanoparticles and nanocomposites in wastewater treatment: Review. *Sustain Mater Technol*, 23 (2020) e00140.

13 Jayaseelan C, Rahuman AA, Kirthi AV, Marimuthu S, Santhosh KT, Bagavan A, Gaurav K, Karthik L & Rao KB, Novel microbial route to synthesize ZnO nanoparticles using *Aeromonas hydrophila* and their activity against pathogenic bacteria and fungi. *Spectrochimica Acta Part A: Mol Biomol Spectrosc*, 90 (2012) 78.

14 Hassani SM, Nakhaei MM & Forghanifard MM, Inhibitory effect of zinc oxide nanoparticles on *Pseudomonas aeruginosa* biofilm formation. *Nanomed J*, 2 (2015) 121.

15 Hameed ASH, Karthikeyan C, Ahamed AP, Thajuddin N, Alharbi NS, Alharbi SA & Ravi G, *In vitro* antibacterial activity of ZnO and Nd doped ZnO nanoparticles against ESBL producing *Escherichia coli* and *Klebsiella pneumoniae*. *Sci Rep*, 6 (2016) 24312.

16 Movahedi F, Masrouri H & Kassaee MZ, Immobilized silver on surface-modified ZnO nanoparticles: As an efficient catalyst for synthesis of propargylamines in water. *J Mol Catal A: Chem*, 395 (2014) 52.

17 Martínková L, Uhnáková B, Pátek M, Nešvera J & Křen V, Biodegradation potential of the genus *Rhodococcus*. *Environ Int*, 35 (2009) 162.

18 Jain N, Bhargava A & Panwar J, Enhanced photocatalytic degradation of methylene blue using biologically synthesized "protein-capped" ZnO nanoparticles. *Chem Eng J*, 243 (2014) 549.

19 Anjum S, Hashim M, Malik SA, Khan M, Lorenzo JM, Abbasi BH & Hano, Recent advances in zinc oxide nanoparticles (ZnO NPs) for cancer diagnosis, target drug delivery, and treatment. *Cancers*, 13 (2021) 4570.

20 Kumar SS, Venkateswarlu P, Rao VR & Rao GN, Synthesis, characterization and optical properties of zinc oxide nanoparticles. *Int Nano Lett*, 3 (2013) 1.

21 Rodrıguez-Paéz JE, Caballero AC, Villegas M, Moure C, Duran P & Fernández JF, Controlled precipitation methods: Formation mechanism of ZnO nanoparticles. *J Eur Ceram Soc*, 21 (2001) 925.

22 Ahmed T, Sadia H, Khalid A, Batool S & Janjua A, Prunes and liver function: A clinical trial. *Pak J Pharm Sci*, 23 (2010) 463.

23 Sultana N, Rehman H, Muntaha ST, Haroon Z, Fatima D & Fakhra H, *Prunus domestica*: A review. *Asian J Pharmacogn*, 4 (2020) 21.

24 Shukla RK, Kishan, Shukla A & Singh R, Evaluation of nutritive value, phytochemical screening, total phenolic content and in-vitro antioxidant activity of the seed of *Prunus domestica* L. *Plant Sci Today,* 8 (2021) 833.

25 Devillers J, Steiman R & Seigle-Murandi F, The usefulness of the agar-well diffusion method for assessing chemical toxicity to bacteria and fungi. *Chemosphere*, 19 (1989) 1693.

26 Amuthavalli P, Hwang JS, Dahms HU, Wang L, Anitha J, Vasanthakumaran M, Gandhi AD, Murugan K, Subramaniam J, Paulpandi M, Chandramohan B & Singh S, Zinc oxide nanoparticles using plant *Lawsonia inermis* and their mosquitocidal, antimicrobial, anticancer applications showing moderate side effects. *Sci Rep*, 11 (2021) 8837.

27 Naseer M, Aslam U, Khalid B & Chen B, Green route to synthesize zinc oxide nanoparticles using leaf extracts of *Cassia fistula* and *Melia azadarach* and their antibacterial potential. *Sci Rep*, 10 (2020) 9055.

28 Venkatesan S, Suresh, S, Arumugam J, Ramu P, Pugazhenthiran N, Jothilakshmi R & Prabu KM, Sunlight-assisted degradation of methylene blue dye by zinc oxide nanoparticles green synthesized using *Vitex negundo* plant leaf extract. *Results Chem*, 7 (2024) 101315.

29 Rohde M, The gram-positive bacterial cell wall. *Microbiol Spectr*, 7 (2019) 1.

30 Decad GM & Nikaido H, Outer membrane of gram-negative bacteria. XII. Molecular sieving function of cell wall. *J Bacteriol*, 128 (1976) 325.

31 Pal A, Pehkonen SO, Liya EY & Ray MB, Photocatalytic inactivation of gram-positive and gram-negative bacteria

using fluorescent light. *J Photochem Photobiol A: Chem*, 186 (2007) 335.

32 Alibi S, Crespo D & Navas J, Plant-derivatives small molecules with antibacterial activity. *Antibiotics*, 10 (2021) 231.

33 Wahab A, Waqas M, Urooj S, Tariq H, Abbasi ZY, Ali M & Abbasi BH, Synthesis of zinc oxide nanoparticles (ZnONPs) from leaf extract of *Carthamus oxycantha* and its in vitro biological applications. *Austin J Anal Pharm Chem*, 10 (2023) 1159.

34 Basnet P, Chanu TI, Samanta D & Chatterjee S, A review on bio-synthesized zinc oxide nanoparticles using plant extracts as reductants and stabilizing agents. *J Photochem Photobiol B: Biol*, 183 (2018) 201.

35 Alamdari S, Sasani GM, Lee C, Han W, Park HH, Tafreshi MJ, Afarideh H & Ara MHM, Preparation and characterization of zinc oxide nanoparticles using leaf extract of *Sambucus ebulus*. *Appl Sci*, 10 (2020) 3620.

36 Arakha M, Roy J, Nayak PS, Mallick B & Jha S, Zinc oxide nanoparticle energy band gap reduction triggers the oxidative stress resulting into autophagy-mediated apoptotic cell death. *Free Radic Biol Med*, 110 (2017) 42.

37 Pai S, Sridevi H, Varadavenkatesan T, Vinayagam R & Selvaraj R, Photocatalytic zinc oxide nanoparticles synthesis using *Peltophorum pterocarpum* leaf extract and their characterization. *Optik*, 185 (2019) 248.

38 Suresh D, Nethravathi PC, Rajanaika H, Nagabhushana H & Sharma SC, Green synthesis of multifunctional zinc oxide (ZnO) nanoparticles using *Cassia fistula* plant extract and their photodegradative, antioxidant and antibacterial activities. *Mat Sci Semicon Proc*, 31 (2015) 446.

39 Ifeanyichukwu UL, Fayemi OE & Ateba CN, Green synthesis of zinc oxide nanoparticles from pomegranate (*Punica granatum*) extracts and characterization of their antibacterial activity. *Molecules*, 25 (2020) 4521.

40 MuthuKathija M, Badhusha MSM & Rama V, Green synthesis of zinc oxide nanoparticles using *Pisonia Alba* leaf extract and its antibacterial activity. *Appl Surf Sci Adv*, 15 (2023) 100400.

41 Pavia DL, Lampman GM, Kriz GS & Vyvyan JR, Spectroscopy, (2011) 8th Indian Reprint.

42 Padalia H, Moteriya P & Chanda S, Synergistic antimicrobial and cytotoxic potential of zinc oxide nanoparticles synthesized using *Cassia auriculata* leaf extract. *Bionanoscience*, 8 (2018) 196.

43 Essalah G, Leroy G, Carru JC, Duponchel B, Mascot M, Poupin C, Guermazi S & Guermazi H, Conduction mechanisms and relaxation phenomena along with electronic transition of $ZnO/ZnNb_2O_6/Nb_2O_5$ composite. *Ceram Int*, 47 (2021) 24732.

44 Kumar S, Bithel N, Kumar S, Kishan, Sen M & Banerjee C, Phyto-mediated synthesis of zinc oxide nanoparticles from *Clerodendrum infortunatum* L. leaf extract and evaluation of antibacterial potential. *S Afr J Bot*, 164 (2024) 146.

45 Sachin, Jaishree, Singh N, Singh R, Shah K & Pramanik BK, Green synthesis of zinc oxide nanoparticles using lychee peel and its application in anti-bacterial properties and CR dye removal from wastewater. *Chemosphere*, 327 (2023) 138497.

46 Aspoukeh PK, Barzinjy AA & Hamad SM, Synthesis, properties and uses of ZnO nanorods: a mini review. *Int Nano Lett*, 12 (2022) 153.

47 Suresh D, Shobharani RM, Nethravathi PC, Kumar MP, Nagabhushana H & Sharma SC, *Artocarpus gomezianus* aided green synthesis of ZnO nanoparticles: Luminescence, photocatalytic and antioxidant properties. *Spectrochim Acta A: Mol Biomol Spectrosc*, 141 (2015) 128.

48 Algarni TS, Abduh NA, Aouissi A & Al-Kahtani A, Photodegradation of methyl orange under solar irradiation on Fe-doped ZnO nanoparticles synthesized using wild olive leaf extract. *Green Process Synth*, 11 (2022) 895.

49 Abdelhakim HK, El-Sayed ER & Rashidi FB, Biosynthesis of zinc oxide nanoparticles with antimicrobial, anticancer, antioxidant and photocatalytic activities by the endophytic *Alternaria tenuissima*. *J Appl Microbiol,* 128 (2020) 1634.

50 Meraat R, Ziabari AA, Issazadeh K, Shadan N & Jalali KM, Synthesis and characterization of the antibacterial activity of zinc oxide nanoparticles against *Salmonella typhi*. *Acta Metall Sin (Engl Lett)*, 29 (2016) 601.

51 Akbar S, Haleem KS, Tauseef I, Rehman W, Ali N & Hasan M, *Raphanus sativus* mediated synthesis, characterization and biological evaluation of zinc oxide nanoparticles. *Nanosci Nanotechnol Lett*, 9 (2017) 2005.

52 Khalid A, Ahmad P, Uddin KM, Modafer Y, Almukhlifi HA, Bazaid AS, Aldarhami A, Alanazi AM, Jefri OA, Uddin MM & Qanash H, Biologically reduced zinc oxide nanosheets using *Phyllanthus emblica* plant extract for antibacterial and dye degradation studies. *J Chem*, 1 (2023) 3971686.